A Simple Method to Automatically Detect Oceanic Eddies

Armando Manuel Fernandes

CENTRIA – Centre for Artificial Intelligence

Universidade Nova Lisboa, Quinta da Torre, 2829-516 Caparica, Portugal

arm.fernandes@gmail.com

Abstract

This paper presents a simple method to detect oceanic eddies in infrared satellite images. The method finds structures that resemble circles or ellipses in binary images. One of its best features is the reduced dependence of its results on the values of input parameters. Its effectiveness is demonstrated for the Iberian Peninsula off-shore region where some methods previously reported on scientific literature are shown to fail. Even though the algorithm effectiveness is demonstrated only for the Iberian Peninsula region its general formulation allows its application to other regions of the world.

1 Introduction

Eddies are mesoscale coherent structures of water presenting nearly symmetrical, rotating circulation patterns (Paillet, 1999). An eddy is shown is Fig. 1(a). They are a fundamental piece of ocean dynamics and have an impact on plankton blooms (Smith *et al.*, 1996), on acoustic wave propagation (Jian *et al.*, 2009), air-sea flux of heat and gas (Vecchi *et al.*, 2004) and global climate (Garabato *et al.*, 2007). In particular, in the region off the Iberian Peninsula oceanographers would like knowing more about the interaction between North Atlantic waters and eddies containing Mediterranean waters (Oliveira *et al.*, 2000). Due to their relevance in the various processes enumerated above, eddies are an interesting research topic.

The research on eddies has been conducted using infrared images from the Advanced Very High Resolution Radiometer (AVHRR) deployed aboard the satellites from the National Oceanographic and Atmospheric Agency (NOAA) (Thonet *et al.*, 1995; Alexanin and Alexanina, 2000; Fernandes and Nascimento, 2006; Fernandes, 2008; Fernandes, 2009). The images containing measurements of radiation in the infrared portion of the spectrum allow to estimate the oceanic surface temperature. The classification by an expert of the large number of these infrared images available is long, fastidious and subjective. Consequently, with the aim of minimising these problems we propose a new method that indicates the regions corresponding to eddies in satellite images. Its advantages when compared to other methods presented in scientific literature are its simplicity and its ability to cope with the low values of the temperature gradients typically found off the Iberian Peninsula. In addition, it has a reduced influence of the parameter values, which is achieved by adding results calculated with different parameter values. The new method we propose allows to obtain lower numbers of false positives than those reported by Fernandes (Fernandes, 2009) for the same eddy detection percentage. This is due to the use of our new false positive reduction procedure.

2 Related Work

In scientific literature one may find various methods to detect eddies in infrared satellite imagery. However up to now, the eddy detection efficiency of many of these methods has not been determined (Nichol, 1987; Guang-Rong *et al.*, 1999; Alexanin and Alexanina, 2000; Yang *et al.*, 2001; Chaudhuri *et al.*, 2004; Ce *et al.*, 2007; Hai *et al.*, 2008; Oram *et al.*, 2008; D'Alimonte, 2009), or has been determined with a small and unrepresentative number of eddies (Peckinpaugh and Holyer, 1994; Torres *et al.*, 2003;

Fernandes and Nascimento, 2006). This prevents the use of these methods for automatic detection, even though they can provide a visual help to the oceanographers carrying out image classification tasks. Since we are interested in developing an automatic eddy detection system we will focus this literature review on works where the detection efficiency has been evaluated on a considerable number of eddies. There are only five works for which this constraint is fulfilled (Thonet *et al.*, 1995; Castellani, 2006; Machado, 2007; Hai *et al.*, 2008; Fernandes, 2009). From these works, those of Castellani (Castellani, 2006) , Machado (Machado, 2007) and Hai *et al.* (Hai *et al.*, 2008) employ neural networks. The work of Castellani presents promising results for the same area that we are interested in, the Iberian Peninsula region. However, in Castellani work only a reduced percentage of the pixels of the satellite images were classified with the neural networks. Recently, Castellani work was continued by Machado (Machado, 2007) that classified complete images. The results show that the neural networks issue too many false positives, which suggests that they are inadequate for the problem in hands. These bad results led us to discard approaches based on neural networks, including the one of Hai *et al.* (Hai *et al.*, 2008), and to focus on other methods in which, contrarily to the neural networks, the system user understands the classification strategy.

We tested Thonet *et al.* (Thonet *et al.*, 1995) method on our images. It was promising because it allowed detecting 81% of a total of 231 eddies, even though issuing 341 false positives. Thonet *et al.* employ a curvature computation to find circular structures that may correspond to an eddy. Once the candidate positions of the eddies is known, a phase portrait is adjusted to the orientation field extracted from the temperatures gradients of the input images. The orientations are like unitary vectors for which the sense is unknown, and so the orientation field allows knowing the ocean water

circulation. From the phase portrait it is possible to know if a certain image region is a spiral and thus an eddy. The centre of the phase portrait, that corresponds to the eddy centres, is then determined. However, using Thonet *et al.* method, we do not obtain an orientation field that adequately describes the water circulation, as depicted in Fig. 1(b), due to the weak temperature gradients in our images. On the other hand, we are able to calculate an orientation field from our method which is described in section 4.4. But, when applying Thonet *et al.* phase-portraits to the orientation field determined with our method it is impossible to calculate a unique centre for the phase-portraits, which prevents their application to the present case, as shown in Fig. 1(c). In summary, we were incapable of successfully applying Thonet *et al.* work to our case.

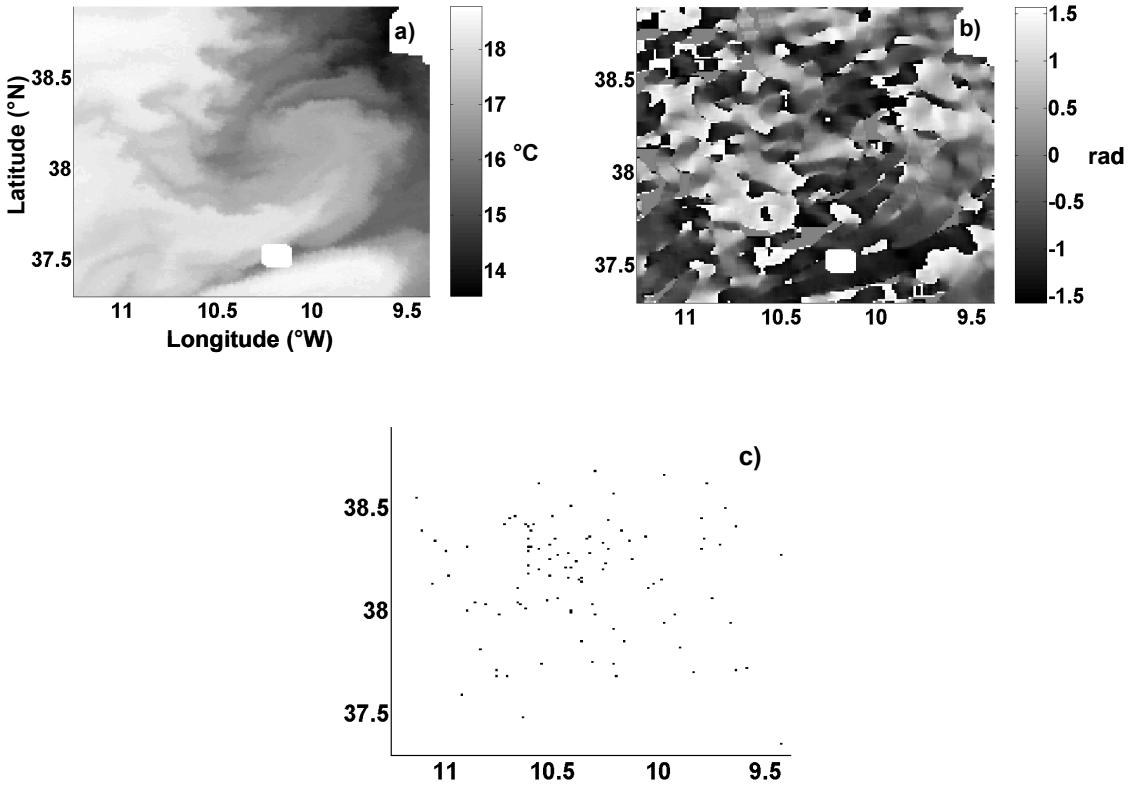

Fig. 1 a) An eddy. b) Orientation field obtained using Thonet *et al.* (Thonet *et al.*, 1995) method. c) Phase-portrait centres obtained employing Thonet *et al.* method together with our orientation field.

The new method we propose allows eliminating an important step from a previous work of the author of the present paper (Fernandes, 2009). That step consists of composing thousands of groups of four to eight points from binary images following rules that allow selecting points that have a high probability of belonging to an ellipse. By eliminating this step the new method becomes significantly faster than the old one, as shown in section 5.2.

3 Images and Eddies Used in the Study

Sixteen brightness temperature maps of the AVHRR were selected for the present study (see Table 1). They contain the measurements of oceanic radiation with wavelengths between 10.3 and 11.3 μm. These wavelengths correspond to channel four of the AVHRR. The area under analysis has latitudes from 33°N to 41°N and longitude between 5°59'49''W and 16°0'51''W. The brightness temperature maps contain 175 eddies that were identified with the help of oceanographers (http://www.io.fc.ul.pt/principal.htm).

The eddies are visible in satellite images as Oliveira *et al.* (Oliveira *et al.*, 2000) demonstrated. They showed that even though eddies have a structure that can be hundreds of meters deep their signature at the ocean surface may be captured in satellite images. The image structures identified as eddies, that were selected for the present study, have shapes compatible with water rotation and present coherent thermal and spatial signature in various brightness temperature maps collected with time gaps that vary from hours up to a few days. These features were also used to select eddies in a previous work of Fernandes (Fernandes, 2009). The importance of analysing the structures' lifetimes has to do with the fact that the most interesting eddies for an

oceanographer are the ones with a large vertical extent and this extent is proportional to the eddy lifetime because a larger water mass withstands longer water mixing.

Map Number	Date in 1998	Satellite Number	Day Number	Hour.Minute
1	24 July	12	205	07.03
2	27 July	14	208	04.07
3	27 July	14	208	15.32
4	28 July	14	209	15.21
5	28 July	12	209	18.34
6	29 July	14	210	03.45
7	29 July	12	210	18.12
8	2 August	14	214	14.26
9	2 August	12	214	18.24
10	3 August	14	215	04.30
11	3 August	12	215	06.42
12	3 August	12	215	18.02
13	4 August	14	216	04.19
14	4 August	12	216	06.20
15	4 August	14	216	14.03
16	4 August	14	216	15.44

Table 1 - Satellite images of the NOAA AVHRR collected in 1998 and used in the present work.

4 Algorithm Description

A diagram of the complete algorithm is shown in Fig. 2

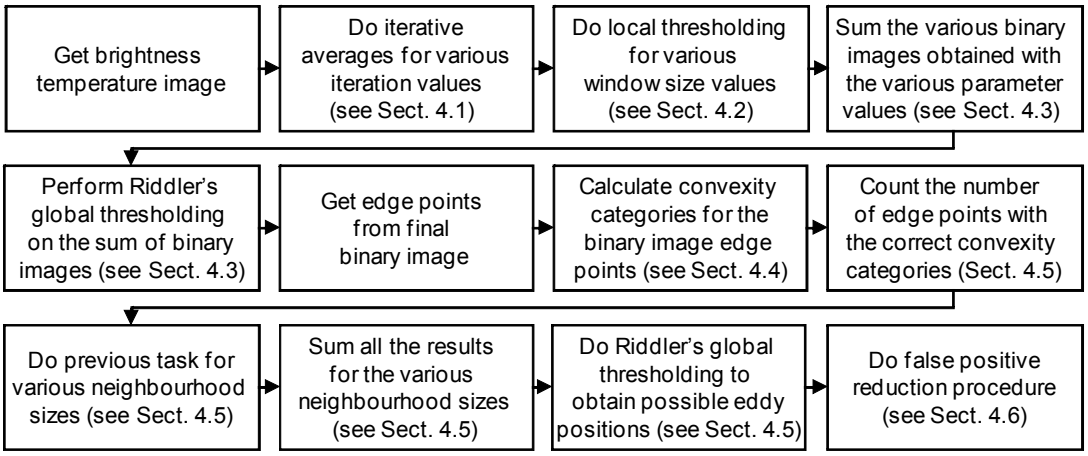

Fig. 2 Diagram of the eddy detection algorithm.

4.1 Iterative Averaging of Temperature Gradients

Our method detects eddies in binary images that contain the edges of the oceanic structures present in brightness temperature maps. To create the binary images it is necessary to calculate an iterative averaging of the temperature gradients (Fernandes, 2008). This iterative averaging is obtained by determining the x and y components of the temperature gradient for each pixel of the brightness temperature map. In our case it is impossible to obtain a continuous eddy outline directly from these gradients because the modulus of the temperature gradients is small and too noisy (Fernandes, 2009). Therefore, it is necessary to calculate an iterative average of the x and y components of the gradient values separately. The iterative average starts with the determination of a new image with the same number of pixels as the original brightness temperature map. The value of each pixel of this new image is the average of the values of the corresponding image pixel, in the original brightness temperature, and of its eight neighbouring pixels. This is the first iteration. Now the result of the first iteration becomes the input for a new average that constitutes a new iteration. The input image of the binarisation procedure consists of the square root of the sum of the squared x and y components of the iterative average obtained after several iterations.

4.2 Image Binarisation

A threshold is calculated for each pixel of the image resulting from the iterative averaging to be used in the creation of the binary images. The binary images will have a value of zero or one if the values of the iterative averaging are below or above the threshold, respectively. The threshold corresponds to the mean of the values of the iterative averaging for all pixels inside a window that contains the pixel for which the threshold is being calculated and its neighbouring pixels. The thresholding based on the

mean value is used due to its simplicity and good results, and was previously employed in Fernandes work (Fernandes, 2008).

4.3 Sum of Binary Images

To carry out the iterative gradient averaging and the image binarisation one must choose the number of iterations and the size of the window used to determine the threshold. The way to minimise the impact of the choice of the value of these parameters on the final eddy detection, is to determine various binary images from various combinations of values of the two parameters and sum the resulting binary images. The final binary image, that is used in eddy detection, is determined with a global thresholding on the sum of the multiple binary images. That image is shown in Fig. 3. The threshold is called global because it is the same for all image pixels. It is calculated using Riddler method (Sezgin and Sankur, 2004) that consists of setting an initial value for the threshold and then iteratively determining a new threshold value. The new threshold value is equal to half the sum of two mean values, one of the values larger, and the other of the values smaller than the previously calculated threshold. New thresholds are iteratively determined in this way until convergence is attained. The threshold value obtained after convergence is the one used to create a binary image.

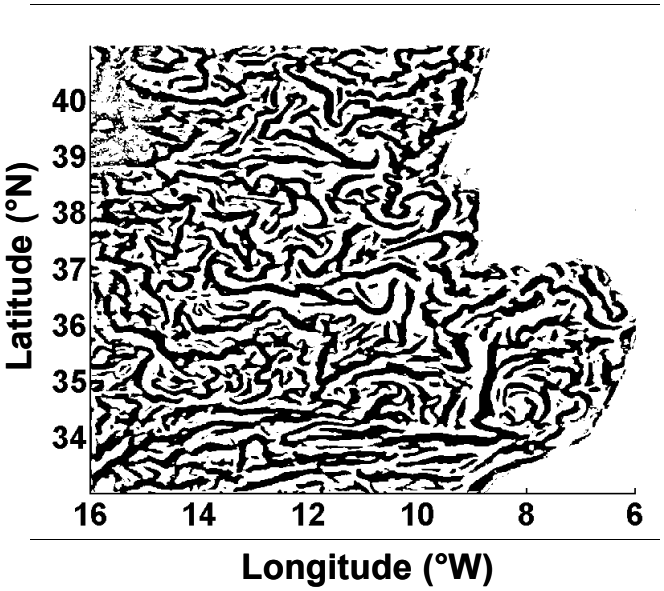

Fig. 3 Final binary image used in eddy detection. It corresponds to the brightness temperature map number 13 from Table 1.

4.4 Convexity Category Determination

A convexity category is assigned to each edge point of the binary image determined in the previous section. This method was employed in other works (Zhang and Liu, 2005; Fernandes, 2008; Fernandes, 2009) There are eight convexity categories, whose representing vectors are illustrated in Fig. 4(a). Each edge point belongs to the category whose representing vector has the closest rotation angle to its convexity vector. The convexity vector of and edge point indicates the concave side of the curve in which the point is positioned, as depicted in Fig. 4(b). That vector is perpendicular to the tangent to the curve at the point under consideration. In practice, to calculate the convexity vector, a second order curve is fitted to the point under analysis and its neighbours, and the tangent is calculated relatively to this second order curve. The coefficients p_0 to p_2 of the second order curve are obtained solving the system (Weisstein, 2009a):

$$\begin{bmatrix} y_1 \\ y_2 \\ \dots \\ y_n \end{bmatrix} = \begin{bmatrix} x_1^2 & x_1 & 1 \\ x_2^2 & x_2 & 1 \\ & \dots & \\ x_n^2 & x_n & 1 \end{bmatrix} \begin{bmatrix} p_2 \\ p_1 \\ p_0 \end{bmatrix}$$

where (x_n,y_n) are the coordinates of the points to fit. In matrix notation:

$$\mathbf{y} = \mathbf{Xp} \Leftrightarrow \mathbf{y} = \mathbf{QRp} \Leftrightarrow \mathbf{p} = \mathbf{R}^{-1}\mathbf{Q}^{\mathrm{T}}\mathbf{y}$$

Matrix **X** is called the Vandermonde matrix (Weisstein, 2009b), matrices **Q** and **R** are the orthogonal and right triangular matrices resulting from the decomposition of **X**, and $\mathbf{R}^{-1}$ is the pseudo-inverse of **R**. The tangent line at point A can be used to define the orientation at point A. These orientations were relevant to test Thonet *et al.* (Thonet *et al.*, 1995) method described in section 2.

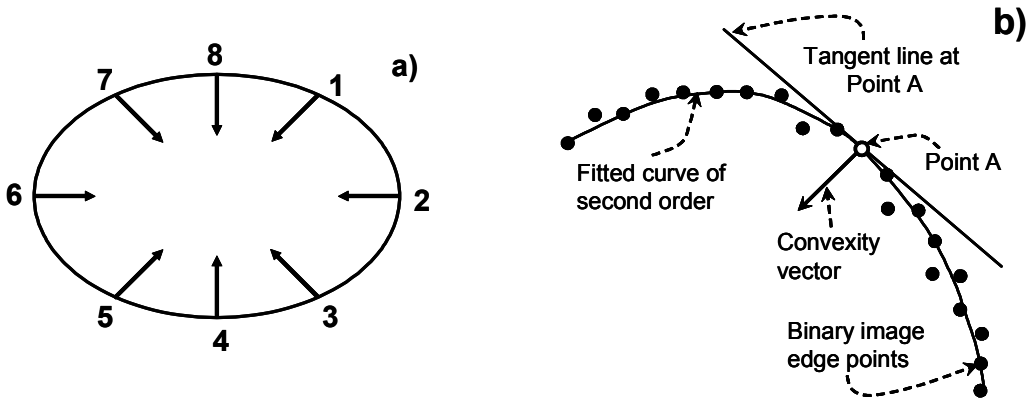

Fig. 4 a) Convexity categories. b) Determination of convexity vector for point A.

4.5 Counting the Number of Edge Points with the Correct Convexity Category

Eddy detection is done assuming that eddies shape is similar to a circle or an ellipse. Consequently, it is done counting, for each pixel of the brightness temperature map, the number of edge points that have the same positions and convexity categories as the points of a virtual circle or ellipse with the pixel under analysis for a centre. In other words, the convexity categories must aim to the pixel under analysis, as depicted in Fig. 5. To make the count one must define a neighbourhood of the pixel under analysis. The size of this neighbourhood is set by the user and is related to the size of the region of influence of each eddy. The result of the pixel count is put in a matrix. That matrix is then normalised by dividing each one of its elements by the sum of the values of all the elements. The matrix with normalised values is called *SumRightConvexities*. The brightness temperature map positions with higher probability of containing an eddy are those corresponding to the matrix *SumRightConvexities* positions with higher values. Since eddies have variable sizes, we must calculate *SumRightConvexities* for several values of the neighbourhood size. A first estimate of eddies positions is given by a matrix named *FinalRightConvexities*, which corresponds to the sum of the various

SumRightConvexities obtained for various neighbourhood sizes. A plot of *FinalRightConvexities* for brightness temperature map number 13 from Table 1 is shown in Fig. 6. The normalisation of *SumRightConvexities* is necessary because the count of the pixels with the right convexities increases with the neighbourhood size, consequently, if the normalisation was not done it would be impossible to detect the smaller eddies in *FinalRightConvexities*.

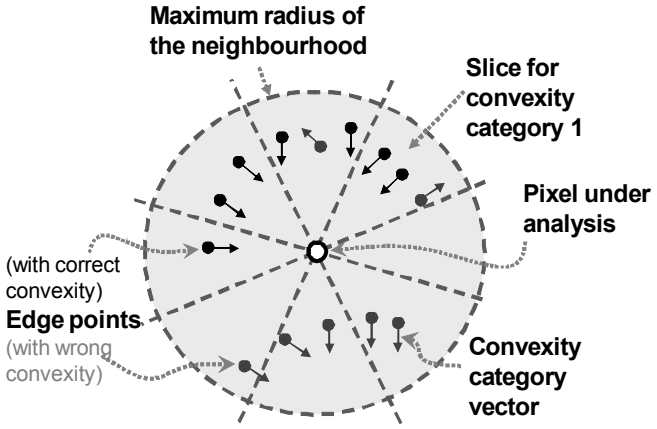

Fig. 5 In black are indicated the binary image edge points with convexity categories that are compatible with circles or ellipses. The number of edge points with the right convexities for the point in the centre of the neighbourhood is seven.

To segment the regions with largest values in matrix *FinalRightConvexities*, which correspond to eddies positions, one must calculate a sequence of thresholds using Riddler's method (Sezgin and Sankur, 2004). In this sequence of thresholds, the first one is calculated using all *FinalRightConvexities* values. The second threshold is calculated by applying Riddler's method to the *FinalRightConvexities* values larger than the first threshold, and so on. A matrix called *BinaryRightConvexities* is then created. In this matrix the values of *FinalRightConvexities* above the third threshold are set to one and the remaining values to zero. The regions with agglomerations of "ones"

surrounded by “zeros” indicate positions where there is a large probability of finding an eddy. The use of the third threshold was determined empirically.

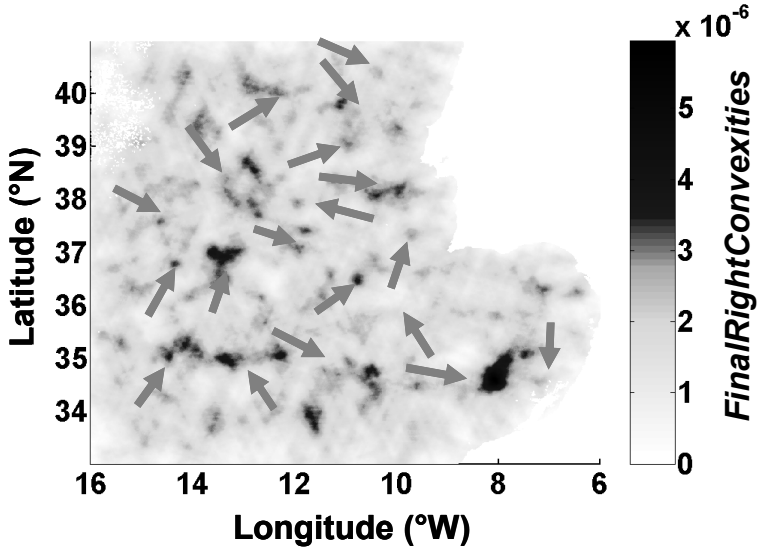

Fig. 6 *FinalRightConvexities* for brightness temperature map number 13 from Table 1. The arrows indicate the position of eddies.

4.6 False Positive Reduction Procedure

To reduce the number of false positives we developed a procedure that employs the *BinaryRightConvexities* matrices of three brightness temperature maps to determine the eddies’ locations in one brightness temperature map. The procedure consists of two pointwise multiplications. One between the *BinaryRightConvexities* matrices corresponding to the brightness temperature map in which we want to find eddies and the previous brightness temperature map available in terms of time. The other multiplication is between the *BinaryRightConvexities* matrices corresponding to the brightness temperature map in which we want to find the eddies and the next brightness temperature map available. The matrices resulting from the multiplications are called *PartialEddyDetectionMatrix* and contain agglomerations of “ones” surrounded by “zeros” in positions where eddies probably exist. The eddies detected in a brightness temperature map correspond to the agglomerations of “ones” in the matrix resulting

from the mathematical *OR* operation between the two *PartialEddyDetectionMatrix*. With this procedure we increase the robustness of the detection process to transient phenomena.

5 Numerical Experiments

5.1 Parameters employed

Each binary image, as described in section 4.3, is created from the sum of 24 binary images. These binary images are the result of combining six values of the number of iterations of the iterative averaging with four sizes of windows of the local thresholding. The number of iterations used was 5, 10, 20, 30, 40 and 50, while the window size was 10, 20, 30 and 40 pixels. We did not use larger numbers of iterations because for values larger than 50, some important outlines of the oceanic structures were not be visible in the resulting binary image. The maximum window size is set so that the window is a bit wider than the thick eddy outlines obtained for 50 iterations. The minimum values of the number of iterations and window size should be close to zero, since that is the case for which the image structures outline is more detailed.

Each matrix *FinalRightConvexities* for each brightness temperature map is determined adding pixelwise eight matrices *SumRightConvexities* calculated with neighbourhood sizes ranging from 30 to 100 pixels in steps of 10 pixels. Even though we have used steps of 10 pixels, because it provides reasonable results, the smaller is the step used, the more accurate the results obtained will be. We went up to 100 pixels to include the complete region of influence of the eddies that is sometimes significantly larger than its core whose radius is around 50 pixels. The *FinalRightConvexities* for values below 30 were not used because they do not seem to contain information relevant for the detection of the eddies present in our brightness temperature maps. For the

determination of the convexity categories of the binary image edge points, 10 points to left and 10 to the right of the edge point under analysis were used in the fitting of the second order curve used to obtain the convexity vectors. This number of pixels is the smallest one that allows obtaining correct convexity categories.

5.2 Results

We estimated the classification efficiency of the new method using the same brightness temperature maps and the same set of eddies employed in previous Fernandes work (Fernandes, 2009). This allows us to compare the results of the old and the new detection methods easily. Without applying the false positive reduction procedure we were able to detect 74% (130/175) of the eddies issuing 179 false positives. Despite the high number of false positives this result is better than random guessing. The reason is that the brightness temperature maps analysed contain 5.3×10^6 pixels corresponding to 678 circular regions with a 50-pixel radius, which is the size expected for the eddy cores. From these circular regions, 175 are eddies and 503 are not. Since the detection percentage, 74%, is superior to the percentage of false positives, 36% (179/503), we may conclude that our system performs better than random guessing. In case of random guessing the two percentages would have approximately the same value. These results are comparable, even though slightly worse than those obtained previously by the author (Fernandes, 2009) where 75% of the eddies were detected at the cost of 162 false positives. In conclusion, the ratio between the number of false positives of the new and old method is 1.1 when the false positive reduction procedure is not used. Using the false positive reduction procedure we propose, we were able to detect 60% of the eddies with 50 false positives which is approximately 10% of the total number of possible false positives. This means that this classification efficiency is also better than random guessing. In addition, it is better than the classification efficiency reported by Fernandes

(Fernandes, 2009) where for an equivalent eddy detection percentage of 58% there were 80 false positives. In this case the ratio of the number of false positives of the new method to the old one is 0.63.

The slight loss of classification efficiency of the new method relatively to the old one, when the false positive reduction procedure is not used is, in our opinion, compensated by the considerably simpler implementation of the new method, which results in a computation time reduction. In fact, in the algorithm reported by Fernandes (Fernandes, 2009) the selection of $5x10^5$ groups of binary image edge points and the determination of ellipse centres takes 161 seconds. In another algorithm (Fernandes, 2008), this same task takes 31 seconds. The equivalent procedure for our new method, which is counting the number of binary image edge points for only one value of the neighbourhood size, takes approximately 2.5 seconds. We make the comparison with only one value of the neighbourhood size because, in the two previous works of Fernandes (Fernandes, 2008; Fernandes, 2009), eddy centres detection was done for only one value of the eddy neighbourhood size. In total, our new method took approximately 3.2 minutes to find eddies in one brightness temperature map. The software was implemented in MATLAB and ran in a Pentium Duo at 3.4 GHz with 1 GB of RAM.

6 Conclusions

We have presented a simple method that allows detecting oceanic eddies. It counts the number of binary image edge points whose vectors, called convexities, have a spatial distribution similar to that of the points of a circle or ellipse. The convexities indicate the concave side of a curve. One of the major advantages of the new method is the reduction of the dependence of the results on the values of input parameters. The eddy detection percentage obtained is 60% with 50 false positives in 16 brightness

temperature maps with 175 eddies, a result that is better than random guessing. The number of false positives, for this eddy detection percentage, is 63% of the number reported in a previous work of the author of the present paper. This reduction of the number of false positives is the consequence of the inclusion of a new step where the information of three brightness temperature maps, instead of only one, is taken into consideration in the eddy detection process. The simplicity of the proposed method allows it to be computationally faster than algorithms reported in previous papers of the author of the present paper. The methods for eddy detection from other authors, whether are not applicable to the regions off the Iberian Peninsula, or are not comparable with the method presented in the current paper as their detection efficiencies were evaluated with a small set of eddies or were not evaluated at all.

7 Acknowledgments

The author would like to thank the Instituto de Oceanografia of Universidade de Lisboa for their expert technical support.

8 References

Alexanin, A. I. and Alexanina, M. G. (2000). Quantitative analysis of thermal sea surface structures on NOAA IR-images. Proceedings of CREAMS. Vladivostok, Russia**:** 158–165.

Castellani, M. (2006). Identification of eddies from sea surface temperature maps with neural networks, International Journal of Remote Sensing 27(8): 1601-1618.

Ce, L., Du, Y. Y., Su, F. Z., Yang, X. M. and Jun, X. (2007). Spatial information recognizing of ocean eddies based on virtual force field and its application, Acta Oceanologica Sinica 26(4): 44-52.

Chaudhuri, A., Gangopadhyay, A., Balasubramanian, R. and Ray, S. (2004). Automated oceanographic feature detection from high resolution satellite images. Proceedings of the Seventh Iasted International Conference on Computer Graphics and Imaging. 217-223.

D'Alimonte, D. (2009). Detection of Mesoscale Eddy-Related Structures Through Iso-SST Patterns, Geoscience and Remote Sensing Letters, IEEE 6(2): 189-193.

Fernandes, A. (2008). Identification of oceanic eddies in satellite images. Proceedings of the International Symposium on Visual Computing, Lecture Notes in Computer Science. G. Bebis. Las Vegas, USA, Springer-Verlag. 5359**:** 65-74.

Fernandes, A. and Nascimento, S. (2006). Automatic water eddy detection in SST maps using random ellipse fitting and vectorial fields for image segmentation, Proceedings of Discovery Science - Lecture Notes in Artificial Intelligence 4265: 77-88.

Fernandes, A. M. (2009). Study on the Automatic Recognition of Oceanic Eddies in Satellite Images by Ellipse Center Detection - The Iberian Coast Case, Geoscience and Remote Sensing, IEEE Transactions on 47(8): 2478-2491.

Garabato, A. C. N., Stevens, D. P., Watson, A. J. and Roether, W. (2007). Short-circuiting of the overturning circulation in the Antarctic Circumpolar Current, Nature 447(7141): 194-197.

Guang-Rong, J., Bao-Liang, L. and Jian, W. (1999). Object searching in scale-space. IEEE International Conference on System, Man and Cybernetics. 1**:** 565-569.

Hai, J., Xiaomei, Y., Jianming, G. and Zhenyu, G. (2008). Automatic eddy extraction from SST imagery using artificial neural network. Congress of the International Society for photogrammetry and Remote Sensing. Beijing. XXXVII-Part B6b**:** 279-282.

Jian, Y. J., Zhang, J., Liu, Q. S. and Wang, Y. F. (2009). Effect of mesoscale eddies on underwater sound propagation, Applied Acoustics 70(3): 432-440.

Machado, G. J. M. (2007). Visualização e análise de vórtices de água em mapas térmicos da superficie oceânica. Master thesis in computer science, Master thesis, Faculdade de Ciências e Tecnologia, Universidade Nova de Lisboa.

Nichol, D. G. (1987). Autonomous Extraction of an Eddy-Like Structure from Infrared Images of the Ocean, Ieee Transactions on Geoscience and Remote Sensing 25(1): 28-34.

Oliveira, P. B., Serra, N., Fiúza, A. F. G. and Ambar, I. (2000). A study of meddies using simultaneous *in situ* and satellite observations. Satellites, Oceanography and Society. D. Halpern. Oceanography Series, Elsevier Science. 63**:** 125-148.

Oram, J. J., McWilliams, J. C. and Stolzenbach, K. D. (2008). Gradient-based edge detection and feature classification of sea-surface images of the Southern California Bight, Remote Sensing of Environment 112(5): 2397-2415.

Paillet, J. (1999). Central water vortices of the eastern North Atlantic, Journal of Physical Oceanography 29(10): 2487-2503.

Peckinpaugh, S. H. and Holyer, R. J. (1994). Circle detection for extracting eddy size and position from satellite imagery of the ocean, IEEE Transactions on Geoscience and Remote Sensing 32(2): 267-273.

Sezgin, M. and Sankur, B. (2004). Survey over image thresholding techniques and quantitative performance evaluation, Journal of Electronic Imaging 13(1): 146-165.

Smith, C. L., Richards, K. J. and Fasham, M. J. R. (1996). The impact of mesoscale eddies on plankton dynamics in the upper ocean, Deep-Sea Research Part I-Oceanographic Research Papers 43(11-12): 1807-1832.

Thonet, H., Lemonnier, B. and Delmas, R. (1995). Automatic segmentation of oceanic eddies on AVHRR thermal infrared sea surface images. Oceans '95 Mts/IEEE - Challenges of Our Changing Global Environment, Conference Proceedings, Vol 2. 1122-1127.

Torres, J., Guindos, F., Peralta, M. and Canton, M. (2003). Competitive neural-net-based system for the automatic detection of oceanic mesoscalar structures on AVHRR scenes, IEEE Transactions on Geoscience and Remote Sensing 41(4): 845-852.

Vecchi, G. A., Xie, S. P. and Fischer, A. S. (2004). Ocean-atmosphere covariability in the western Arabian Sea, Journal of Climate 17(6): 1213-1224.

Weisstein, E. W. (2009a). Least squares fitting-polynomial, MathWorld-A Wolfram Web Resource, http://mathworld.wolfram.com/LeastSquaresFittingPolynomial.html,

Weisstein, E. W. (2009b). Vandermonde matrix, MathWorld-A Wolfram Web Resource, http://mathworld.wolfram.com/VandermondeMatrix.html,

Yang, Q., Parvin, B. and Mariano, A. (2001). Detection of vortices and saddle points in SST data, Geophysical Research Letters 28(2): 331-334.

Zhang, S. C. and Liu, Z. Q. (2005). A robust, real-time ellipse detector, Pattern Recognition 38(2): 273-287.